

Optical Noise of Dual-State Lasing Quantum Dot Lasers

Yueguang Zhou¹, Member, IEEE, Jianan Duan², Member, IEEE, Frédéric Grillot, Senior Member, IEEE, and Cheng Wang³, Member, IEEE

Abstract—This paper theoretically investigates the optical noise characteristics of the simultaneous ground-state (GS) and excited-state (ES) lasing quantum dot lasers. The optical noise dynamics of both states are analysed through coupling the Langevin noise sources into a set of coupled rate equations. It is pointed out that the ES emission significantly changes the evolution scenario of the relative intensity noise, the frequency noise (spectral linewidth), and the linewidth broadening factor of the GS emission, as a function of the bias current. In the vicinity of the ES lasing threshold, the relative intensity noise and the frequency noise of the GS emission is lower than those of ES emission. However, the linewidth broadening factor of the GS emission is larger than the latter.

Index Terms—Semiconductor lasers, quantum dots, relative intensity noise, frequency noise, spectral linewidth, linewidth broadening factor.

I. INTRODUCTION

QUANTUM dot (QD) lasers are silicon-compatible laser sources for developing photonic integrated circuits (PICs), which is witnessing rapid growth driven by the increasing demands for 5G infrastructures, high speed optical interconnects in data centers and LIDAR for self-driving automobiles [1], [2]. Thanks to the low sensitivity of QDs to the epitaxial growth defects [3], [4], the steady-state performances of QD lasers epitaxially grown on silicon are becoming comparable to their counterparts grown on the native GaAs or InP substrate, including the low threshold current density and the high temperature stability [3]–[6]. QD lasers also exhibit low optical noise characteristics, including both relative intensity noise (RIN) and frequency noise (FN) [7]–[10]. It has been shown that the RIN of QD lasers reached down to -160 dB/Hz [7], [11], [12], and the record spectral linewidth was as low as

60 kHz [8]. In addition, QD lasers are highly tolerant to optical feedback, owing to the large damping factor and/or small linewidth broadening factor (LBF) [10], [13], [14], which are significantly beneficial for isolator-free integration in silicon-based PICs.

In addition to the usual ground-state (GS) emission, QD lasers can also emit solely on the excited state (ES), or simultaneously on both states [15]–[19]. The ES-lasing QD lasers usually exhibit higher modulation bandwidth than that of GS-lasing ones, owing to the faster carrier relaxation rate and higher differential gain [16], [17], [20], [21]. In addition, the ES emission shows a smaller LBF than the GS emission [21], [22]. However, the ES-lasing QD lasers are found to be more sensitive to the optical feedback due to the smaller damping rate [22], [23]. On the other hand, dual-state lasing in QD lasers enhances the modulation bandwidth as well [19], [24]. Interestingly, dual-state laser emission exhibits lower intensity noise than sole GS or ES emission, which is attributed to the quasi-antiphase dynamics through the carrier relaxation process. [25]. Optical feedback usually triggers mode switching or mode competition between the GS and the ES [26], [27], while feedback with finely controlled phase is helpful to reduce the RIN of two-state lasing QD laser [28]. However, the QD laser operated at the ES lasing threshold is very sensitive to the optical feedback [29]. Recently, Xiong and Zhang theoretically proved that the phonon bottleneck effect and the inhomogeneous broadening effect play crucial roles on the dual-state lasing behavior [30].

In this work, we theoretically investigate the optical noise characteristics of InAs/InP QD lasers emitting simultaneously on the GS and the ES. We present a dual-state lasing QD rate equation model including all the Langevin noise sources. Increasing the bias current generally reduces the RIN and the spectral linewidth of the GS emission, except at the ES lasing threshold. However, the ES emission is found to significantly change the evolution scenario of the GS emission noise, with respect to the bias current. We also analyze the optical noise characteristics of ES emission, which show monotonic reduction with increasing bias currents. It is shown that in the vicinity of the ES lasing threshold, the optical noise of ES emission is higher than that of GS emission. Finally, through the analysis of FN spectra, we obtain LBFs of the GS emission and the ES emission, respectively. Below the ES lasing threshold, raising the bias current increases the LBF of the GS emission. Above the ES lasing threshold, however,

Manuscript received June 17, 2020; revised August 29, 2020; accepted September 17, 2020. Date of publication September 23, 2020; date of current version October 6, 2020. This work was supported in part by the National Natural Science Foundation of China under Grant 61804095 and in part by the Shanghai Natural Science Foundation under Grant 20ZR1436500. (Corresponding author: Cheng Wang.)

Yueguang Zhou and Cheng Wang are with the School of Information Science and Technology, ShanghaiTech University, Shanghai 201210, China (e-mail: wangcheng1@shanghaitech.edu.cn).

Jianan Duan is with the LTCI, Télécom Paris, Institut Polytechnique de Paris, 91120 Palaiseau, France (e-mail: jianan.duan@telecom-paristech.fr).

Frédéric Grillot is with the LTCI, Télécom Paris, Institut Polytechnique de Paris, 91120 Palaiseau, France, and also with the Center for High Technology Materials, The University of New Mexico, Albuquerque, NM 87106 USA (e-mail: grillot@telecom-paristech.fr).

Color versions of one or more of the figures in this article are available online at <http://ieeexplore.ieee.org>.

Digital Object Identifier 10.1109/JQE.2020.3026090

0018-9197 © 2020 IEEE. Personal use is permitted, but republication/redistribution requires IEEE permission. See <https://www.ieee.org/publications/rights/index.html> for more information.

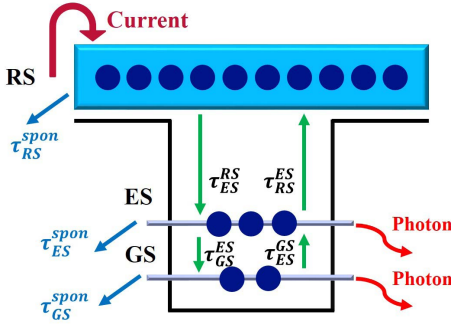


Fig. 1. The schematic of carrier dynamics in a QD laser.

the LBF of the GS emission is reduced while the LBF of the ES emission is almost constant. The paper is organized as follows: In Section II, we introduce the rate equation model of dual-state lasing InAs/InP QD lasers, as well as its linearized form in the frequency domain. Section III discusses the dual-state lasing characteristics including the RIN, the FN, and the LBF. Section IV summarizes this work.

II. RATE EQUATION MODEL OF DUAL-STATE LASING QD LASERS

Figure 1 illustrates the schematic of the carrier dynamics in QD lasers [21], [31]. It is assumed that the active region consists of only one ensemble, that is, all the QDs have the same size. Therefore, the inhomogeneous effect due to the dot size dispersion is not considered in this work. The QD laser is simplified as a three-level system: a two-dimensional carrier reservoir (RS), a four-fold degenerate ES, and a two-fold degenerate GS, where the electron-hole pairs are treated as neutral excitons. Carriers are injected directly from the electrodes to the RS, followed by a capture process into the ES with a capture time τ_{ES}^{RS} . Finally, carriers relax into the GS with a relaxation time τ_{GS}^{ES} . It is noted that the direct carrier capture process from the RS to the GS is neglected, which otherwise can accelerate the carrier scattering rate to the GS [32]. However, the incorporation of the direct carrier capture channel will not affect the conclusion of this work. On the other hand, due to the thermal excitation, some carriers are excited from the GS to the ES with a time τ_{ES}^{GS} , and from the ES to the RS with a time τ_{RS}^{ES} , respectively. Carriers in all the three states recombine spontaneously with times $\tau_{RS,ES,GS}^{spon}$, respectively. Both the GS and the ES exhibit stimulated emission simultaneously. Dynamics of the carrier numbers $N_{RS,ES,GS}$, the photon numbers $S_{ES,GS}$, and the phases of the two electric fields $\phi_{ES,GS}$ are expressed as:

$$\frac{dN_{RS}}{dt} = \frac{I}{q} + \frac{N_{ES}}{\tau_{RS}^{ES}} - \frac{N_{RS}}{\tau_{ES}^{RS}}(1 - \rho_{ES}) - \frac{N_{RS}}{\tau_{RS}^{spon}} + F_{RS} \quad (1)$$

$$\begin{aligned} \frac{dN_{ES}}{dt} = & \left(\frac{N_{RS}}{\tau_{RS}^{ES}} + \frac{N_{GS}}{\tau_{ES}^{GS}} \right) (1 - \rho_{ES}) - \frac{N_{ES}}{\tau_{ES}^{RS}}(1 - \rho_{GS}) \\ & - \frac{N_{ES}}{\tau_{RS}^{ES}} - \Gamma_p v_g g_{ES} S_{ES} - \frac{N_{ES}}{\tau_{ES}^{spon}} + F_{ES} \end{aligned} \quad (2)$$

$$\begin{aligned} \frac{dN_{GS}}{dt} = & \frac{N_{ES}}{\tau_{GS}^{ES}}(1 - \rho_{GS}) - \frac{N_{GS}}{\tau_{ES}^{GS}}(1 - \rho_{ES}) \\ & - \Gamma_p v_g g_{GS} S_{GS} - \frac{N_{GS}}{\tau_{GS}^{spon}} + F_{GS} \end{aligned} \quad (3)$$

$$\frac{dS_{ES}}{dt} = \left(\Gamma_p v_g g_{ES} - \frac{1}{\tau_p} \right) S_{ES} + \beta_{sp} \frac{N_{ES}}{\tau_{ES}^{spon}} + F_{S_{ES}} \quad (4)$$

$$\frac{dS_{GS}}{dt} = \left(\Gamma_p v_g g_{GS} - \frac{1}{\tau_p} \right) S_{GS} + \beta_{sp} \frac{N_{GS}}{\tau_{GS}^{spon}} + F_{S_{GS}} \quad (5)$$

$$\frac{d\phi_{ES}}{dt} = \frac{1}{2} \Gamma_p v_g (g_{GS} \kappa_{ES}^{GS} + g_{ES} \alpha_{ES} + g_{RS} \kappa_{ES}^{RS}) + F_{\phi_{ES}} \quad (6)$$

$$\frac{d\phi_{GS}}{dt} = \frac{1}{2} \Gamma_p v_g (g_{GS} \alpha_{GS} + g_{ES} \kappa_{GS}^{ES} + g_{RS} \kappa_{GS}^{RS}) + F_{\phi_{GS}} \quad (7)$$

where I is the injected current, q is the elementary charge, and $\rho_{ES,GS}$ are the carrier occupation probabilities in each state [33]. τ_p is the photon lifetime, Γ_p is the optical confinement factor, β_{sp} is the spontaneous emission factor, and v_g is the group velocity of the light. $\alpha_{ES,GS}$ are self-contributions of the carrier population in the ES, GS to the LBF of ES, GS, respectively. $\kappa_{ES}^{RS,GS}$ are cross-contributions of carrier population in the RS, GS to the LBF of ES, respectively. $\kappa_{GS}^{RS,ES}$ are cross-contributions of carrier population in the RS, ES to the LBF of GS, respectively. $g_{ES,GS}$ are material gains of each state, which are expressed as [33]:

$$g_{ES} = \frac{a_{ES}}{1 + \zeta_{ES} \frac{S_{ES}}{V_S}} \frac{N_B}{V_B} (2\rho_{ES} - 1) \quad (8)$$

$$g_{GS} = \frac{a_{GS}}{1 + \zeta_{GS} \frac{S_{GS}}{V_S}} \frac{N_B}{V_B} (2\rho_{GS} - 1) \quad (9)$$

where $a_{ES,GS}$ are the differential gains, and $\zeta_{ES,GS}$ are the gain compression factors of each state. N_B is the total number of QDs, V_B is the volume of the active region, and V_S is the volume occupied by the photons in the laser cavity. g_{RS} is the RS gain [33].

The carrier noise and the spontaneous emission noise are characterized by the Langevin approach [34]. $F_{RS,ES,GS}$ are the carrier noise sources in each state. $F_{S_{ES,GS}}$ are the photon noise sources of spontaneous emission, and $F_{\phi_{ES,GS}}$ are the phase noise sources of spontaneous emission. Both the carrier noise and the spontaneous emission noise are white noise, and hence the expectation values of all the above Langevin noise sources are zero. The auto- and cross-correlations of all the noise sources are given by:

$$\langle F_i(t) F_j(t') \rangle = U_{i,j} \delta(t - t') \quad (10)$$

where i, j are representing $RS, ES, GS, S_{ES}, S_{GS}, \phi_{ES}$, and ϕ_{GS} . The correlation coefficients $U_{i,j}$ are derived using the classical method described in [34], and non-zero coefficients are given by (11)-(18):

$$U_{RS,RS} = 2 \times \left[\frac{N_{RS}}{\tau_{RS}^{ES}} (1 - \rho_{ES}) + \frac{N_{RS}}{\tau_{RS}^{spon}} \right] \quad (11)$$

$$U_{ES,ES} = 2 \times \left[\left(\frac{N_{RS}}{\tau_{RS}} + \frac{N_{GS}}{\tau_{GS}} \right) (1 - \rho_{ES}) - \Gamma_p v_g g_{ES} S_{ES} + \beta_{sp} \frac{N_{ES}}{\tau_{ES}^{spont}} S_{ES} \right] \quad (12)$$

$$U_{GS,GS} = 2 \times \left[\frac{N_{ES}}{\tau_{ES}} (1 - \rho_{GS}) - \Gamma_p v_g g_{GS} S_{GS} + \beta_{sp} \frac{N_{GS}}{\tau_{GS}^{spont}} S_{GS} \right] \quad (13)$$

$$U_{S_{ES(GS)}, S_{ES(GS)}} = 2 \times \beta_{sp} \frac{N_{ES(GS)}}{\tau_{ES(GS)}^{spont}} S_{ES(GS)} \quad (14)$$

$$U_{\phi_{ES(GS)}, \phi_{ES(GS)}} = \frac{1}{2 S_{ES(GS)}} \beta_{sp} \frac{N_{ES(GS)}}{\tau_{ES(GS)}^{spont}} \quad (15)$$

$$U_{RS,ES} = - \left[\frac{N_{RS}}{\tau_{RS}} (1 - \rho_{ES}) + \frac{N_{ES}}{\tau_{RS}} \right] \quad (16)$$

$$\gamma_{11} = \frac{1 - \rho_{ES}}{\tau_{RS}^{RS}} + \frac{1}{\tau_{RS}^{spont}}; \gamma_{12} = \frac{1}{\tau_{RS}^{ES}} + \frac{1}{4N_B} \frac{N_{RS}}{\tau_{RS}^{RS}};$$

$$\gamma_{21} = \frac{1 - \rho_{ES}}{\tau_{RS}^{RS}};$$

$$\gamma_{22} = \frac{1 - \rho_{GS}}{\tau_{ES}^{ES}} + \frac{1}{\tau_{RS}^{ES}} + \frac{1}{\tau_{ES}^{spont}} + \frac{1}{4N_B} \left(\frac{N_{RS}}{\tau_{RS}^{RS}} + \frac{N_{GS}}{\tau_{GS}^{RS}} \right) + \frac{1}{2} \Gamma_p v_g a_{ES} S_{ES}; \gamma_{23} = \frac{1 - \rho_{ES}}{\tau_{ES}^{GS}} + \frac{1}{2N_B} \frac{N_{ES}}{\tau_{GS}^{ES}};$$

$$\gamma_{24} = -\Gamma_p v_g g_{ES} + \Gamma_p v_g a_{PES} S_{ES};$$

$$\gamma_{32} = \frac{1 - \rho_{GS}}{\tau_{GS}^{ES}} + \frac{1}{4N_B} \frac{N_{GS}}{\tau_{GS}^{RS}};$$

$$\gamma_{33} = \frac{1 - \rho_{ES}}{\tau_{ES}^{GS}} + \frac{1}{\tau_{GS}^{spont}} + \frac{1}{2N_B} \frac{N_{ES}}{\tau_{GS}^{ES}} + \Gamma_p v_g a_{GS} S_{GS};$$

$$\gamma_{35} = -\Gamma_p v_g g_{GS} + \Gamma_p v_g a_{PGS} S_{GS};$$

$$\gamma_{42} = \frac{1}{2} \Gamma_p v_g a_{ES} S_{ES} + \frac{\beta_{sp}}{\tau_{ES}^{spont}};$$

$$\gamma_{44} = \frac{1}{\tau_p} - \Gamma_p v_g g_{ES} + \Gamma_p v_g a_{PES} S_{ES};$$

$$\gamma_{53} = \Gamma_p v_g a_{GS} S_{GS} + \frac{\beta_{sp}}{\tau_{GS}^{spont}};$$

$$\gamma_{55} = \frac{1}{\tau_p} - \Gamma_p v_g g_{GS} + \Gamma_p v_g a_{PGS} S_{GS};$$

$$\gamma_{61} = \Gamma_p v_g a_{RS} \kappa_{ES}^{RS}; \gamma_{62} = \frac{1}{4} \Gamma_p v_g a_{ES} \alpha_{ES}$$

$$\gamma_{63} = \frac{1}{2} \Gamma_p v_g a_{GS} \kappa_{ES}^{GS}; \gamma_{64} = -\frac{1}{2} \Gamma_p v_g a_{PES} \alpha_{ES};$$

$$\gamma_{65} = -\frac{1}{2} \Gamma_p v_g a_{PGS} \kappa_{ES}^{GS}; \gamma_{71} = \Gamma_p v_g a_{RS} \kappa_{GS}^{RS};$$

$$\gamma_{72} = \frac{1}{4} \Gamma_p v_g a_{ES} \kappa_{GS}^{ES}; \gamma_{73} = \frac{1}{2} \Gamma_p v_g a_{GS} \alpha_{GS};$$

$$\gamma_{74} = -\frac{1}{2} \Gamma_p v_g a_{PES} \kappa_{GS}^{ES}; \gamma_{75} = -\frac{1}{2} \Gamma_p v_g a_{PGS} \alpha_{GS}; \quad (20)$$

Through standard small signal analysis of the rate equations (1)-(7), the linearized rate equations in the frequency domain is derived in (19) and the matrix components are expressed

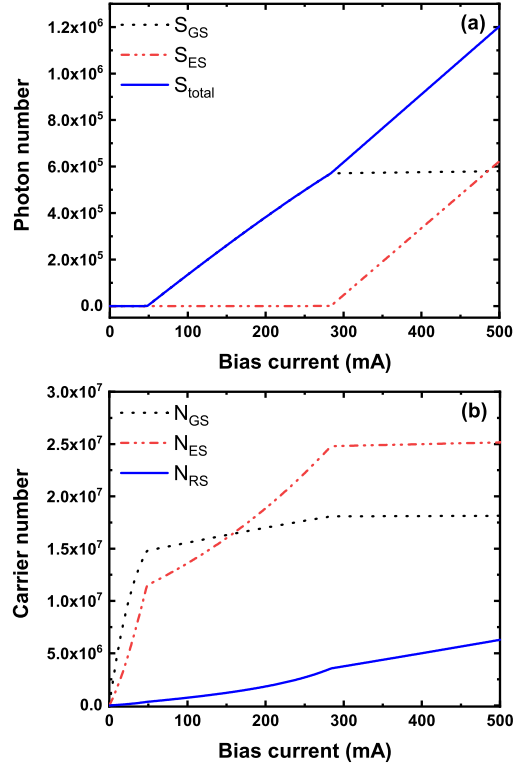


Fig. 2. (a) Photon numbers emitted from the GS, the ES, and their summation. (b) Carrier numbers of GS, ES and RS as a function of the bias current. $I_{th}^{GS} = 49$ mA, $I_{th}^{ES} = 284$ mA.

in (20). In the small signal analysis, the gain compression effect is approximated by considering $a_{PES,GS}$ with $dg_{ES,GS} = a_{ES,GS} dN_{ES,GS} - a_{PES,GS} dS_{ES,GS}$ [34]. Applying Cramer's rule, small-signal variations of the carrier number δN , the photon number δS , and the phase $\delta\phi$ can be obtained. The RIN and the FN of each lasing state are defined as:

$$RIN(\omega)_i = \left| \frac{\delta S_i(\omega)}{S_i} \right|^2 \quad (21)$$

$$FN(\omega)_i = \left| \frac{j\omega}{2\pi} \delta\phi_i(\omega) \right|^2 \quad (22)$$

with i being ES and GS, ω being the angular frequency, S being the average photon number, $\delta S(\omega)$ being the photon number variation, and $\delta\phi(\omega)$ being the phase variation. The laser under study is an InAs/InP QD laser, and the laser parameters used for the simulations are listed in Table I [21], [31]. It is worthwhile to mention that the optical confinement factor is dependent on the QD density, the number of stacked QD layers, and the structure of cladding layer [35]–[37]. The value of the optical confinement factor used in the simulation is 0.06 [38].

III. RESULTS AND DISCUSSION

Figure 2(a) depicts S_{GS} , S_{ES} , and the total photon number S_{total} as a function of the bias current. The GS lasing threshold is $I_{th}^{GS} = 49$ mA, and the ES one is $I_{th}^{ES} = 284$ mA. Above the ES lasing threshold, the slope efficiency of the GS emission significantly decreases, which is smaller than that of the ES emission. On the other hand, the slope efficiency of the total laser emission slightly increases. This behavior is consistent

TABLE I
MATERIAL AND OPTICAL PARAMETERS OF THE QD LASER

Symbol	Description	Value
E_{RS}	RS transition energy	0.97 eV
E_{ES}	ES transition energy	0.87 eV
E_{GS}	GS transition energy	0.82 eV
τ_{ES}^{RS}	RS to ES capture time	6.3 ps
τ_{GS}^{ES}	ES to GS relaxation time	2.9 ps
τ_{RS}^{ES}	ES to RS escape time	2.7 ns
τ_{ES}^{GS}	GS to ES escape time	10.4 ps
τ_{RS}^{spon}	RS spontaneous emission time	0.5 ns
τ_{ES}^{spon}	ES spontaneous emission time	0.5 ns
τ_{GS}^{spon}	GS spontaneous emission time	1.2 ns
τ_p	Photon lifetime	4.1 ps
T_2	Polarization dephasing time	0.1 ps
β_{sp}	Spontaneous emission factor	5.0×10^{-6}
a_{GS}	GS Differential gain	$5.0 \times 10^{-15} \text{ cm}^2$
a_{ES}	ES Differential gain	$10 \times 10^{-15} \text{ cm}^2$
ξ_{ES}	ES Gain compression factor	$1.0 \times 10^{-15} \text{ cm}^3$
ξ_{GS}	GS Gain compression factor	$1.0 \times 10^{-15} \text{ cm}^3$
Γ_p	Optical confinement factor	0.06
α_{GS}	intrinsic α -factor of GS	0.50
α_{ES}	intrinsic α -factor of ES	0.50
κ_{ES}^{RS}	RS to ES contribution coefficient	0.059
κ_{ES}^{GS}	GS to ES contribution coefficient	-0.137
κ_{GS}^{RS}	RS to GS contribution coefficient	0.037
κ_{GS}^{ES}	ES to GS contribution coefficient	0.122
N_B	Total dot number	1.0×10^7
D_{RS}	Total RS state number	4.8×10^6
V_B	Active region volume	$5.0 \times 10^{-11} \text{ cm}^3$
V_{RS}	RS region volume	$1.0 \times 10^{-11} \text{ cm}^3$
R	Mirror reflectivity	0.32
α_i	Internal modal loss	6.0 cm^{-1}
n	Refractive index	3.5
N	QD layer number	5
L	Cavity length	0.5 mm
W	Cavity width	$4.0 \mu\text{m}$

with the experimental observation in [32]. In Fig. 2(b), both N_{GS} and N_{ES} have clear kinks at both lasing thresholds.

The above-threshold N_{ES} is higher than the above-threshold N_{GS} , due to the larger degeneracy of the ES. Both carriers are not completely clamped but slightly increased with increasing bias current. This is due to the gain compression effect, which is characterized by the gain compression factor in (8) and (9). Increasing the photon number reduces the effective differential gain, and hence more carrier populations (or higher carrier occupation probabilities) are demanded to maintain a constant gain value, which is governed by the cavity loss [34]. On the other hand, the RS carrier number N_{RS} is much smaller than N_{GS} and N_{ES} for all the bias currents.

A. Relative Intensity Noise Characteristics

Figure 3(a) shows the RIN of the GS emission (RIN_{GS}) at several bias currents. Below the ES lasing threshold, RIN_{GS} shows a clear resonance peak, and the resonance frequency increases with the bias current as expectation. Meanwhile, increasing the bias current reduces the whole RIN spectrum. Above the ES lasing threshold, the resonance peak of RIN_{GS} is almost completely suppressed. The RIN evolution of the ES emission (RIN_{ES}) in Fig. 3(b) is similar as RIN_{GS} below the ES lasing threshold. However, the resonance frequency of RIN_{ES} is about 3 times larger than the latter, which leads to the higher modulation bandwidth of the ES emission as observed in [16], [21].

Figure 4 depicts the low-frequency (at 1.0 MHz) RINs of both GS and ES emissions as a function of the bias current. Below the ES lasing threshold, RIN_{GS} decreases rapidly from -126.3 dB/Hz at $1.2 \times I_{th}^{GS}$ down to -154.9 dB/Hz at $5.2 \times I_{th}^{GS}$. However, at the ES lasing threshold, RIN_{GS} abruptly increases to -149.4 dB/Hz. This significant increase of RIN_{GS} is in agreement with the experimental observation in [25]. The high RIN_{GS} can be attributed to the large optical power fluctuations induced by the strong spontaneous emission of the ES, due to the coupling of the GS and the ES through the carrier relaxation process [25]. Beyond the ES lasing threshold, RIN_{GS} reduces slightly, and becomes almost constant around -155 dB/Hz. On the other hand, RIN_{ES} significantly decreases from -135.4 dB/Hz at $1.1 \times I_{th}^{ES}$ to -156.8 dB/Hz at $2.0 \times I_{th}^{ES}$.

$$U_{ES,GS} = - \left[\frac{N_{GS}}{\tau_{ES}} (1 - \rho_{ES}) + \frac{N_{ES}}{\tau_{GS}} (1 - \rho_{GS}) \right] \quad (17)$$

$$U_{ES(GS),S_{ES(GS)}} = - \left[2\beta_{sp} \frac{N_{ES(GS)}}{\tau_{ES(GS)}^{spon}} S_{ES(GS)} - \Gamma_p v_g g_{ES(GS)} S_{ES(GS)} \right] \quad (18)$$

$$\begin{bmatrix} \gamma_{11} + j\omega & -\gamma_{12} & 0 & 0 & 0 & 0 & 0 \\ -\gamma_{21} & \gamma_{22} + j\omega & -\gamma_{23} & -\gamma_{24} & 0 & 0 & 0 \\ 0 & -\gamma_{32} & \gamma_{33} + j\omega & 0 & -\gamma_{35} & 0 & 0 \\ 0 & -\gamma_{42} & 0 & \gamma_{44} + j\omega & 0 & 0 & 0 \\ 0 & 0 & -\gamma_{53} & 0 & \gamma_{55} + j\omega & 0 & 0 \\ -\gamma_{61} & -\gamma_{62} & -\gamma_{63} & -\gamma_{64} & -\gamma_{65} & j\omega & 0 \\ -\gamma_{71} & -\gamma_{72} & -\gamma_{73} & -\gamma_{74} & -\gamma_{75} & 0 & j\omega \end{bmatrix} \times \begin{bmatrix} \delta N_{RS} \\ \delta N_{ES} \\ \delta N_{GS} \\ \delta S_{ES} \\ \delta S_{GS} \\ \delta \phi_{ES} \\ \delta \phi_{GS} \end{bmatrix} = \begin{bmatrix} F_{RS} \\ F_{ES} \\ F_{GS} \\ F_{S_{ES}} \\ F_{S_{GS}} \\ F_{\phi_{ES}} \\ F_{\phi_{GS}} \end{bmatrix} \quad (19)$$

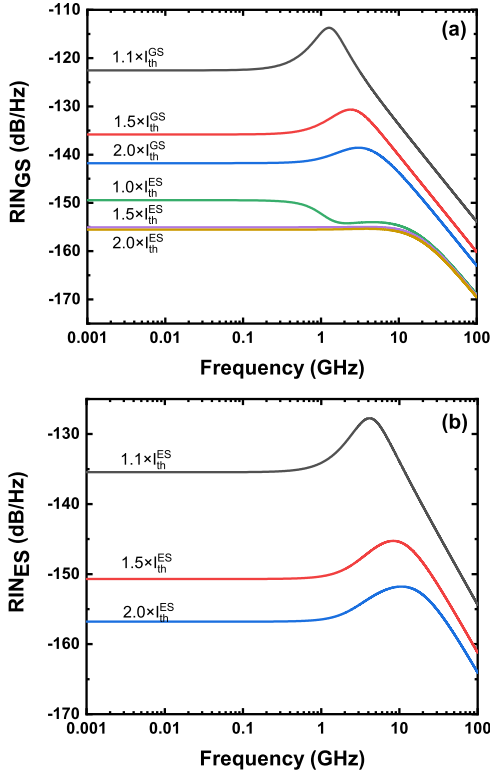


Fig. 3. RIN spectra of laser emitted from (a) the GS and (b) the ES at several bias currents. $I_{th}^{ES} \approx 5.8 \times I_{th}^{GS}$.

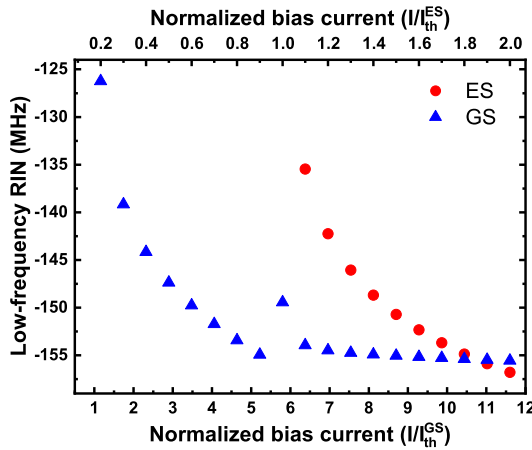


Fig. 4. Low-frequency RINs at 1 MHz of GS emission and ES emission as a function of the normalized bias current.

B. Frequency Noise Characteristics

Figure 5(a) shows that the FN of the GS emission (FN_{GS}) generally decreases with increasing bias current, and the resonance peak is suppressed. However, at the ES lasing threshold, the low frequency part of FN_{GS} is significantly increased, due to the high LBF described in Fig. 7. The FN of the ES emission (FN_{ES}) in Fig. 5(b) shows similar evolution as FN_{GS} below the ES lasing threshold.

From the low-frequency value of the FN spectrum, we obtain the intrinsic linewidth of semiconductor lasers through the simple relation $\Delta\nu_{OL} = 2\pi FN|_{f=1.0 \text{ MHz}}$ [33], [39]. The intrinsic linewidth is determined by both the

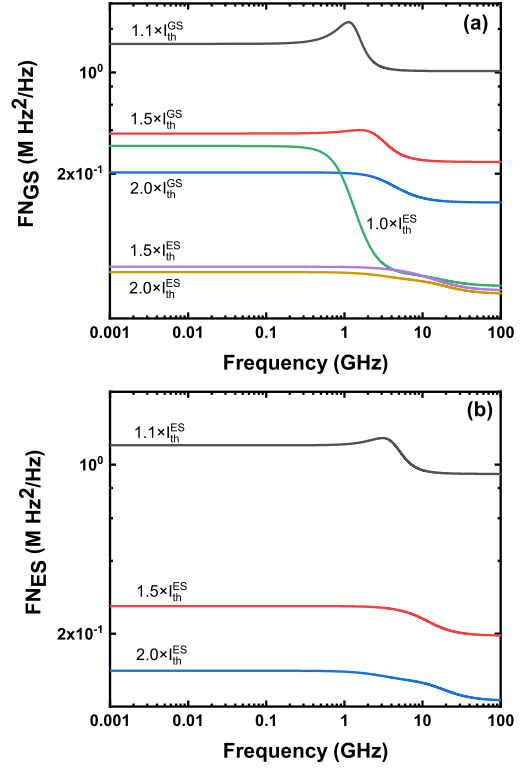


Fig. 5. FN spectra of laser emissions from (a) the GS and (b) the ES at several bias currents. $I_{th}^{ES} \approx 5.8 \times I_{th}^{GS}$.

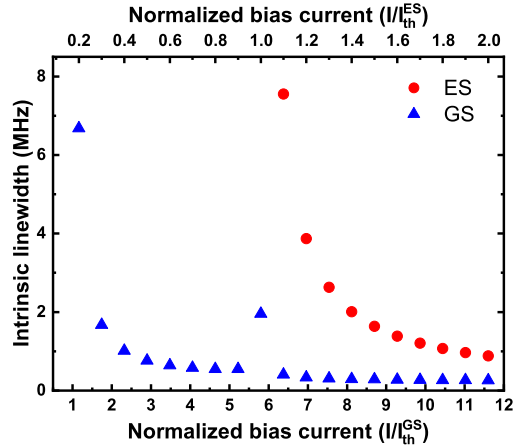


Fig. 6. Intrinsic linewidths of GS emission and ES emission as a function of the normalized bias current.

spontaneous emission noise and the LBF [34]. It is noted that the rate equations do not take into account technical noise sources including current source noise, temperature fluctuation, and mechanical vibration, which can significantly raise the low-frequency FN. Figure 6 depicts that the intrinsic linewidth of the GS emission decreases from 6.7 MHz at $1.2 \times I_{th}^{GS}$ down to 0.5 MHz at $5.2 \times I_{th}^{GS}$. At the ES lasing threshold, the intrinsic linewidth exhibits an abrupt increase to 2.0 MHz as the low-frequency RIN in Fig. 4. Above the ES lasing threshold, the intrinsic linewidth of the GS becomes almost constant around 0.26 MHz. Meanwhile, the intrinsic linewidth of the ES emission declines from 7.6 MHz at $1.1 \times I_{th}^{ES}$ to 0.88 MHz at $2.0 \times I_{th}^{ES}$.

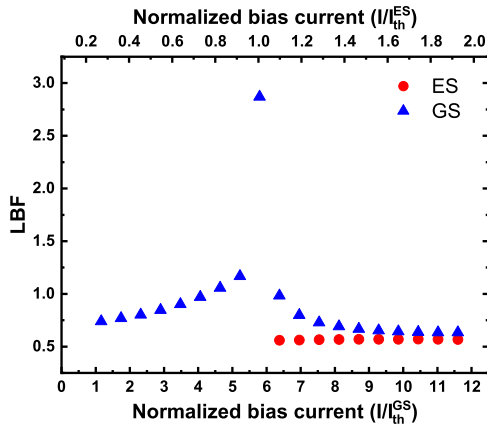


Fig. 7. LBFs of the GS and the ES as a function of the normalized bias current.

On the other hand, from the high-frequency value of the FN spectrum, the Schawlow-Townes linewidth of semiconductor lasers is extracted through $\Delta\nu_{ST} = 2\pi FN|_{(f=100 \text{ GHz})}$. The intrinsic linewidth $\Delta\nu_{OL}$ of semiconductor lasers is broadened by the LBF from the Schawlow-Townes linewidth $\Delta\nu_{ST}$ as

$$\Delta\nu_{OL} = \Delta\nu_{ST}(1 + a^2) \quad (23)$$

Using the above formula, Fig. 7 extracts the LBFs of both the GS and the ES. Below the ES lasing threshold, the LBF of the GS increases from 0.7 at $1.2 \times I_{th}^{GS}$ to 1.2 at $5.2 \times I_{th}^{GS}$, due to the increased contribution of carrier variations in the ES and in the RS [21], [33]. At the ES lasing threshold, the LBF dramatically increases to 2.9, due to the strong carrier perturbation induced by the onset of ES emission. This increased LBF results in the poor resistance to optical feedback at the ES lasing threshold, as experimentally observed in [29]. Interestingly, the LBF of the GS becomes declining for bias currents above the ES lasing threshold. This phenomenon is qualitatively in good agreement with the experimental observation in [40], where a giant LBF is observed around the ES threshold. The LBF reduction can be attributed to the stimulated emission of the ES, which stabilizes the carrier vibration induced by the spontaneous emission, because the stimulated emission consumes much more carriers than the spontaneous emission [41]. On the other hand, the LBF of the ES is almost constant around 0.57, which is slightly smaller than the LBF of the GS for the same bias current.

IV. CONCLUSION

In summary, we propose a rate equation model of dual-state lasing InAs/InP QD lasers including the Langevin noise sources, which enables the investigation of RIN and FN dynamics. The RIN and the intrinsic linewidth of both GS emission and ES emission generally decrease with increasing bias current. However, at the ES lasing threshold, both the low-frequency RIN and the linewidth of the GS emission abruptly increase. Beyond the ES lasing threshold, both become almost constant. In addition, it is found that the LBF of the GS increases with bias current below the ES lasing threshold, while becomes decreasing when it is above the ES threshold. Interestingly, the QD laser exhibits a giant LBF at the ES lasing threshold. On the other hand, the LBF of the ES is also

almost constant, which is slightly smaller than the GS one. The findings in this work suggest that the ES emission in QD lasers hardly degrades the noise performance of the GS emission, except at the ES lasing threshold. Therefore, practical applications of QD lasers should avoid current operation in the vicinity of the ES threshold. Finally, although the simulations in this work are based on InAs/InP lasers, we believe that the conclusions are also suitable for InAs/GaAs dual-state emission QD lasers, which can be obtained by replacing the parameters in Table I with the InAs/GaAs ones.

REFERENCES

- [1] J. C. Norman *et al.*, "A review of high-performance quantum dot lasers on silicon," *IEEE J. Quantum Electron.*, vol. 55, no. 2, pp. 1–11, Apr. 2019.
- [2] J. C. Norman, D. Jung, Y. Wan, and J. E. Bowers, "Perspective: The future of quantum dot photonic integrated circuits," *APL Photon.*, vol. 3, no. 3, Mar. 2018, Art. no. 030901.
- [3] S. Chen *et al.*, "Electrically pumped continuous-wave III–V quantum dot lasers on silicon," *Nature Photon.*, vol. 10, no. 5, pp. 307–311, 2016.
- [4] A. Y. Liu *et al.*, "Electrically pumped continuous-wave 1.3 μm quantum-dot lasers epitaxially grown on on-axis (001) GaP/Si," *Opt. Lett.*, vol. 42, no. 2, pp. 338–341, 2017.
- [5] Y. Wang *et al.*, "Monolithic quantum-dot distributed feedback laser array on silicon," *Optica*, vol. 5, no. 5, pp. 528–533, 2018.
- [6] S. Zhu, B. Shi, Q. Li, and K. M. Lau, "1.5 μm quantum-dot diode lasers directly grown on CMOS-standard (001) silicon," *Appl. Phys. Lett.*, vol. 113, no. 22, 2018, Art. no. 221103.
- [7] M. Liao *et al.*, "Low-noise 1.3 μm InAs/GaAs quantum dot laser monolithically grown on silicon," *Photon. Res.*, vol. 6, no. 11, pp. 1062–1066, 2018.
- [8] T. Septon *et al.*, "Large linewidth reduction in semiconductor lasers based on atom-like gain material," *Optica*, vol. 6, no. 8, pp. 1071–1077, 2019.
- [9] J. Duan, H. Huang, Z. G. Lu, P. J. Poole, C. Wang, and F. Grillot, "Narrow spectral linewidth in InAs/InP quantum dot distributed feedback lasers," *Appl. Phys. Lett.*, vol. 112, no. 12, Mar. 2018, Art. no. 121102.
- [10] J. Duan *et al.*, "Dynamic and nonlinear properties of epitaxial quantum dot lasers on silicon for isolator-free integration," *Photon. Res.*, vol. 7, no. 11, pp. 1222–1228, 2019.
- [11] A. Capua *et al.*, "Direct correlation between a highly damped modulation response and ultra low relative intensity noise in an InAs/GaAs quantum dot laser," *Opt. Express*, vol. 15, no. 9, pp. 5388–5393, 2007.
- [12] F. Lelarge *et al.*, "Recent advances on InAs/InP quantum dash based semiconductor lasers and optical amplifiers operating at 1.55 μm ," *IEEE J. Sel. Topics Quantum Electron.*, vol. 13, no. 1, pp. 111–124, Feb. 2007.
- [13] J. Duan *et al.*, "Semiconductor quantum dot lasers epitaxially grown on silicon with low linewidth enhancement factor," *Appl. Phys. Lett.*, vol. 112, no. 25, Jun. 2018, Art. no. 251111.
- [14] Y.-G. Zhou, X.-Y. Zhao, C.-F. Cao, Q. Gong, and C. Wang, "High optical feedback tolerance of InAs/GaAs quantum dot lasers on germanium," *Opt. Express*, vol. 26, no. 21, pp. 28131–28139, 2018.
- [15] A. Markus, J. X. Chen, C. Paranthoen, A. Fiore, C. Platz, and O. Gauthier-Lafaye, "Simultaneous two-state lasing in quantum-dot lasers," *Appl. Phys. Lett.*, vol. 82, no. 12, pp. 1818–1820, Mar. 2003.
- [16] B. J. Stevens, D. T. D. Childs, H. Shahid, and R. A. Hogg, "Direct modulation of excited state quantum dot lasers," *Appl. Phys. Lett.*, vol. 95, no. 6, Aug. 2009, Art. no. 061101.
- [17] D. Arsenijević *et al.*, "Comparison of dynamic properties of ground- and excited-state emission in p-doped InAs/GaAs quantum-dot lasers," *Appl. Phys. Lett.*, vol. 104, no. 18, May 2014, Art. no. 181101.
- [18] A. Rohm, B. Lingnau, and K. Ludge, "Understanding ground-state quenching in quantum-dot lasers," *IEEE J. Quantum Electron.*, vol. 51, no. 1, pp. 1–11, Jan. 2015.
- [19] A. Röhlm, B. Lingnau, and K. Ludge, "Ground-state modulation-enhancement by two-state lasing in quantum-dot laser devices," *Appl. Phys. Lett.*, vol. 106, no. 19, May 2015, Art. no. 191102.
- [20] P.-F. Xu, H.-M. Ji, J.-L. Xiao, Y.-X. Gu, Y.-Z. Huang, and T. Yang, "Reduced linewidth enhancement factor due to excited state transition of quantum dot lasers," *Opt. Lett.*, vol. 37, no. 8, pp. 1298–1300, 2012.
- [21] C. Wang, B. Lingnau, K. Ludge, J. Even, and F. Grillot, "Enhanced dynamic performance of quantum dot semiconductor lasers operating on the excited state," *IEEE J. Quantum Electron.*, vol. 50, no. 9, pp. 1–9, Sep. 2014.

- [22] H. Huang, D. Arsenijević, K. Schires, T. Sadeev, D. Bimberg, and F. Grillot, "Multimode optical feedback dynamics of InAs/GaAs quantum-dot lasers emitting on different lasing states," *AIP Adv.*, vol. 6, no. 12, Dec. 2016, Art. no. 125114.
- [23] L.-C. Lin *et al.*, "Comparison of optical feedback dynamics of InAs/GaAs quantum-dot lasers emitting solely on ground or excited states," *Opt. Lett.*, vol. 43, no. 2, pp. 210–213, 2018.
- [24] Z.-R. Lv *et al.*, "Dynamic characteristics of two-state lasing quantum dot lasers under large signal modulation," *AIP Adv.*, vol. 5, no. 10, Oct. 2015, Art. no. 107115.
- [25] R. Pawlus, L. L. Colombo, P. Bardella, S. Breuer, and M. Gioannini, "Intensity noise behavior of an InAs/InGaAs quantum dot laser emitting on ground states and excited states," *Opt. Lett.*, vol. 43, no. 4, pp. 867–870, 2018.
- [26] M. Virte, K. Panajotov, and M. Sciamanna, "Mode competition induced by optical feedback in two-color quantum dot lasers," *IEEE J. Quantum Electron.*, vol. 49, no. 7, pp. 578–585, Jul. 2013.
- [27] M. Virte, S. Breuer, M. Sciamanna, and K. Panajotov, "Switching between ground and excited states by optical feedback in a quantum dot laser diode," *Appl. Phys. Lett.*, vol. 105, no. 12, Sep. 2014, Art. no. 121109.
- [28] R. Pawlus, S. Breuer, and M. Virte, "Relative intensity noise reduction in a dual-state quantum-dot laser by optical feedback," *Opt. Lett.*, vol. 42, no. 21, pp. 4259–4262, 2017.
- [29] H. Huang *et al.*, "Analysis of the optical feedback dynamics in InAs/GaAs quantum dot lasers directly grown on silicon," *J. Opt. Soc. Amer. B, Opt. Phys.*, vol. 35, no. 11, pp. 2780–2787, 2018.
- [30] Y. Xiong and X. Zhang, "Two-state lasing at room temperature in InAs/InP quantum dots," *J. Appl. Phys.*, vol. 126, no. 13, Oct. 2019, Art. no. 133102.
- [31] C. Wang, F. Grillot, and J. Even, "Impacts of wetting layer and excited state on the modulation response of quantum-dot lasers," *IEEE J. Quantum Electron.*, vol. 48, no. 9, pp. 1144–1150, Sep. 2012.
- [32] K. Veselinov *et al.*, "Analysis of the double laser emission occurring in 1.55- μm InAs-InP (113) B quantum-dot lasers," *IEEE J. Quantum Electron.*, vol. 43, no. 9, pp. 810–816, Sep. 2007.
- [33] C. Wang, J.-P. Zhuang, F. Grillot, and S.-C. Chan, "Contribution of off-resonant states to the phase noise of quantum dot lasers," *Opt. Express*, vol. 24, no. 26, pp. 29872–29881, 2016.
- [34] L. A. Coldren, S. W. Corzine, and M. L. Mashanovitch, *Diode Lasers and Photonic Integrated Circuits*. Hoboken, NJ, USA: Wiley, 2012.
- [35] D. Bimberg, M. Grundmann, and N. N. Ledentsov, *Quantum Dot Heterostructures*. Hoboken, NJ, USA: Wiley, 1999.
- [36] P. G. Eliseev *et al.*, "Ground-state emission and gain in ultralow-threshold InAs-InGaAs quantum-dot lasers," *IEEE J. Sel. Topics Quantum Electron.*, vol. 7, no. 2, pp. 135–142, Mar./Apr. 2001.
- [37] M. V. Maximov *et al.*, "A 1.33 μm InAs/GaAs quantum dot laser with a 46 cm^{-1} modal gain," *Semicond. Sci. Technol.*, vol. 23, no. 10, 2008, Art. no. 1050042.
- [38] Y. N. M. Sugawara, K. Mukai, and H. Ishikawa, "Effect of homogeneous broadening of optical gain on lasing spectra in self-assembled $\text{In}_x\text{Ga}_{1-x}\text{As/GaAs}$ quantum dot lasers," *Phys. Rev. B, Condens. Matter*, vol. 61, no. 11, pp. 7595–7603, 2000.
- [39] J. Duan, X.-G. Wang, Y.-G. Zhou, C. Wang, and F. Grillot, "Carrier-noise-enhanced relative intensity noise of quantum dot lasers," *IEEE J. Quantum Electron.*, vol. 54, no. 6, pp. 1–7, Dec. 2018.
- [40] B. Dagens *et al.*, "Giant linewidth enhancement factor and purely frequency modulated emission from quantum dot laser," *Electron. Lett.*, vol. 41, no. 6, pp. 323–324, Mar. 2005.
- [41] F. Grillot, B. Dagens, J.-G. Provost, H. Su, and L. F. Lester, "Gain compression and above-threshold linewidth enhancement factor in 1.3- μm InAs-GaAs quantum-dot lasers," *IEEE J. Quantum Electron.*, vol. 44, no. 10, pp. 946–951, Oct. 2008.

Yueguang Zhou (Member, IEEE) was born in Lianyuan, China, in 1995. He received the bachelor's degree in electronic science and technology from the Harbin Institute of Technology, Harbin, China, in 2017. He is currently pursuing the master's degree with ShanghaiTech University. His research mainly focuses on the theoretical modeling and experimental characterization of the dynamics of quantum dot lasers grown on germanium/silicon.



Jianan Duan (Member, IEEE) was born in Yinchuan, China, in 1992. He received the B.S. degree in optronics engineering from the Huazhong University of Science and Technology, China, in 2014, and the M.S. degree and the Ph.D. degree in optoelectronics from the University of Paris-Saclay, France, in 2016 and 2019, respectively. He is currently a Post-Doctoral Researcher with Télécom Paris, Institut Polytechnique de Paris, France. His current research interests are focused on theoretical modeling, experimental characterization and optimization of quantum dot lasers for applications in fiber-optic communication networks, and in photonic integrated circuits. He had been awarded the Best Ph.D. Theses Award funded by Mines-Telecom Foundation in 2020.



Frédéric Grillot (Senior Member, IEEE) was born in Versailles, France, in August 1974. He received the M.Sc. degree in physics from the University of Dijon, France, in 1999, the Ph.D. degree in electrical engineering from the University of Besançon, France, in 2003, and the Research Habilitation degree in physics from the University of Paris VII, France, in 2012. His Ph.D. research activities were conducted with the Optical Component Research Department, Nokia Bell Laboratories (formerly Alcatel-Lucent), working on the effects of the optical feedback dynamics in semiconductor lasers, and the impact of this phenomenon on communication systems. From 2003 to 2004, he was with the Center for Nanoscience and Nanotechnology (C2N), University Paris-Saclay, where he focused on integrated optics modeling and silicon-based passive devices for optical interconnects. From 2004 to 2012, he was an Assistant Professor with the Institut National des Sciences Appliquées (INSA), Rennes, France. From 2008 to 2009, he was a Visiting Research Professor with The University of New Mexico, Albuquerque, NM, USA, leading research in optoelectronics at the Center for High Technology Materials (CHTM). In October 2012, he joined Télécom Paristech one of the top French public institutions of higher education and research of engineering, France, as an Associate Professor and became a Full Professor in January 2017. Since August 2015, he has also been serving as a Research Professor with The University of New Mexico. From April 2017 to December 2017, he joined the Electrical Engineering Department, University of California Los Angeles (UCLA), Los Angeles, CA, USA, as a Visiting Professor teaching dynamics of lasers and applied quantum mechanics. He has published 103 journal articles, 1 book, 3 book chapters, and more than 200 contributions in international conferences and workshops. His current research interests include, but are not limited to, advanced quantum confined devices using new materials, such as quantum dots and dashes, light emitters based on intersubband transitions, nonlinear dynamics, and optical chaos in semiconductor lasers systems, as well as microwave and silicon photonics applications. He is currently serving as an Associate Editor for *Optics Express* (OSA) and a Senior Consultant and Advisor Technology Partnerships for Baehl Innovation. He is a fellow of the SPIE and a Senior Member of the IEEE Photonics Society and the Optical Society of America (OSA).



Cheng Wang (Member, IEEE) was born in Tengzhou, China, in 1987. He received the M.S. degree in physical electronics from the Harbin Institute of Technology, Harbin, China, in 2011, and the Ph.D. degree in optoelectronics from the Institut National des Sciences Appliquées (INSA), Rennes, France, in 2015. During his Ph.D. period, he has researched at Télécom ParisTech, France, Technische Universität Berlin, Germany, and the Politecnico di Torino, Italy, respectively. Then, he joined the Department of Electronic Engineering, City University of Hong Kong, Hong Kong, as a Senior Research Assistant. Since 2016, he has been an Assistant Professor with ShanghaiTech University, Shanghai, China. His main research interests include modeling and characterization of quantum structured semiconductor lasers, including quantum dot lasers, quantum cascade lasers, and interband cascade lasers, for applications in optical communication, and in gas spectroscopy.